First-order phase transitions in two-dimensional off-lattice liquid crystals

2007 J. Phys.: Condens. Matter 19 466109

(http://iopscience.iop.org/0953-8984/19/46/466109)

IOP PUBLISHING JOURNAL OF PHYSICS: CONDENSED MATTER

J. Phys.: Condens. Matter **19** (2007) 466109 (20pp) doi:10.1088/0953-8984/19/46/466109

First-order phase transitions in two-dimensional off-lattice liquid crystals

H H Wensink and R L C Vink

Institut für Theoretische Physik II: Weiche Materie, Heinrich-Heine-Universität Düsseldorf, Universitätsstraße 1, D-40225 Düsseldorf, Germany

Received 31 August 2007, in final form 9 October 2007
Published 26 October 2007
Online at stacks.iop.org/JPhysCM/19/466109

Abstract

We consider an *off-lattice* liquid crystal pair potential in strictly two dimensions. The potential is purely repulsive and short ranged. Nevertheless, by means of a single parameter in the potential, the system is shown to undergo a first-order phase transition. The transition is studied using mean-field density functional theory, and shown to be of the isotropic-to-nematic kind. In addition, the theory predicts a large density gap between the two coexisting phases. The first-order nature of the transition is confirmed using computer simulation and finite-size scaling. Also presented is an analysis of the interface between the coexisting domains, including estimates of the line tension, as well as an investigation of anchoring effects.

1. Introduction

The phase behaviour of liquid crystals in two dimensions continues to be an interesting topic. On the one hand, at least for *lattice* liquid crystals, there is a clear resemblance to the planar spin or XY-model [1]. In fact, the Lebwohl–Lasher (LL) model [2], which is one of the standard liquid crystal models, maps exactly onto the XY-model in two dimensions. The XY-model does not support long-range order [3] and, consequently, long-range nematic order is believed to be absent in many two-dimensional (2D) liquid crystals as well [4–6]. In addition, the XY-model features a Kosterlitz–Thouless (KT) transition [7, 8]. Consequently, phase transitions in two-dimensional liquid crystals are often interpreted in terms of the KT scenario [9, 10, 6, 4, 5]. In particular, the KT transition is a *continuous* transition, as opposed to first order. As a result, the possibility of a first-order transition occurring in a two-dimensional liquid crystal has received relatively little attention.

Interestingly, computer simulations of appropriately *generalized* XY-models have shown that the possibility of a first-order transition also occurring in these systems should be taken seriously [11–13]. More recently, these findings were put on firm mathematical ground by

van Enter and Shlosman [14–16]. In particular, it was demonstrated that Hamiltonians of the form

$$\mathcal{H}_{\mathrm{gXY}} = -\sum_{\langle i,j\rangle}\left(\frac{1+\hat{\omega}_i\cdot\hat{\omega}_j}{2}\right)^p, \tag{1}$$

undergo first-order phase transitions when p is large [16]. In equation (1), the sum is over nearest neighbours on a square lattice, and $\hat{\omega}_i$ are two-dimensional unit vectors. The usual XY-model (up to a trivial constant and multiplicative factor) is recovered for $p = 1$; the generalization is to also consider $p \gg 1$. In computer simulations, the first-order transition was already observed at $p = 50$ [11]. Of course, for small p, the KT scenario is ultimately recovered again, for which the transition is continuous.

The results obtained for generalized XY-models have similar consequences for two-dimensional liquid crystals. This was recently demonstrated in [17] using a generalized version of the LL model

$$\mathcal{H}_{gLL} = -\sum_{\langle i,j\rangle}|\hat{\omega}_i\cdot\hat{\omega}_j|^p, \tag{2}$$

the essential difference from equation (1) being inversion symmetry under $\hat{\omega}_i \leftrightarrow -\hat{\omega}_i$ of the particle orientations. In particular, it was shown that equation (2) undergoes a first-order temperature-driven transition, from an isotropic to a quasi-nematic phase, provided p is sufficiently large. Again, the threshold value is at $p \approx 50$ [17]. In the isotropic phase, the orientational correlations decay exponentially; in the quasi-nematic phase, they decay algebraically. Both phases thus lack long-range order in the thermodynamic limit, in agreement with the Mermin–Wagner theorem [3]. Consequently, the nematic order parameter cannot be used to describe the first-order transition in equation (2). Instead, a valid order parameter is the energy density, which shows a 'jump' at the transition temperature. By keeping the energy density fixed at some value in the coexistence region, phase coexistence between isotropic and quasi-nematic domains can be realized [17].

The aim of this paper is to investigate how robust these findings are when *off-lattice* liquid crystals in two dimensions are also considered. To this end, we formulate an *off-lattice* model of a liquid crystal, which is somewhat inspired by the lattice Hamiltonian of equation (2). The model will be presented in section 2. Next, the phase behaviour of this model is studied, using theory and simulation. Indeed, both the theory and the simulation find strong evidence for the existence of a first-order transition, including a pronounced coexistence region. The coexistence region will be analysed in some detail, including estimates of the line tension between the coexisting domains. An important improvement over the lattice model of equation (2) is that the transition in the *off-lattice* model is characterized by a 'jump' in the particle density. In other words, phase coexistence can now be studied by keeping the overall particle density fixed at some appropriate value, rather than the energy density. This finding is relevant for possible experiments, where the condition of fixed density is rather easy to implement (in contrast, keeping the overall energy fixed in an experiment would be much more difficult). At the same time, we find that the analogue of the p-exponent in equation (2) must be quite large before the first-order transition begins to show up. Whether such 'sharp' interactions can be realized experimentally is not yet clear, but some suggestions are made toward the end of this paper.

2. Off-lattice liquid crystal in two dimensions

In this paper, we consider an ensemble of particles, whose positions and orientations are confined to a two-dimensional plane. The particles interact with each other via a pair potential

v_{ij} of the form

$$v_{ij} = \epsilon\sigma_{ij}\left(1 - |\hat{\omega}_i \cdot \hat{\omega}_j|^p\right) u(r), \tag{3}$$

$$\sigma_{ij} = 1 + \nu\left[(\hat{\omega}_i \cdot \mathbf{r}_{ij}/r)^2 + (\hat{\omega}_j \cdot \mathbf{r}_{ij}/r)^2\right], \tag{4}$$

with $\mathbf{r}_{ij} = \mathbf{r}_j - \mathbf{r}_i$, $r = |\mathbf{r}_{ij}|$, $-1/2 < \nu < 1/2$, and coupling parameter $\epsilon > 0$. In what follows, factors of $k_\mathrm{B}T$ are absorbed into the parameter ϵ, with T the temperature, and k_B the Boltzmann constant. The quantity $\hat{\omega}_i$ is a two-dimensional unit vector denoting the orientation of the ith particle; $\mathbf{r}_i$ is a two-dimensional vector denoting the coordinate of the centre-of-mass of the ith particle. The radial function $u(r)$ in equation (3) is assumed to be strictly positive and short ranged. Here, we take a simple step function

$$u(r) = \begin{cases} 1 & r < a, \\ 0 & \text{otherwise}, \end{cases} \tag{5}$$

with a the particle diameter, which will henceforth serve as our unit of length.

As for the lattice Hamiltonian of equation (2), the potential is constructed such that inversion symmetry is maintained. Note also that v_{ij} is purely repulsive. Nevertheless, we expect a first-order phase transition to take place, either at low temperature or at high density, provided p is large. The purpose of the parameter ν is to introduce a coupling between the orientational and translational degrees of freedom. By setting $\nu = 0$, no such coupling occurs, and the potential becomes separable. For this special case, Straley has rigorously proved the absence of long-range nematic order [18]. As far as we know, the absence or presence of long-range order for the case $\nu \neq 0$ is still an open question.

3. Density functional theory

In this section, we use density functional theory (DFT) to study the *off-lattice* 2D liquid crystal model of equation (3). Within DFT the thermodynamics and structure of a fluid is described by a functional $\Omega[\rho]$ of the one-particle distribution $\rho(\mathbf{r}, \hat{\omega})$. The density functional is such that it is minimized for a given (μ, A, T) by the equilibrium one-particle distribution and the minimum value of the functional is the grand potential [19] (in the present study in two dimensions, A is the system area). Here we use a simple mean-field functional, which, in the absence of an external potential, can be cast in the following form:

$$\Omega[\rho] = \int \mathrm{d}\mathbf{r}\,\mathrm{d}\hat{\omega}\,\rho(\mathbf{r}, \hat{\omega})\left(\ln[\mathcal{V}\rho(\mathbf{r}, \hat{\omega})] - 1 - \mu\right) + \tfrac{1}{2}\int \mathrm{d}\mathbf{r}\,\mathrm{d}\hat{\omega}\int \mathrm{d}\mathbf{r}'\,\mathrm{d}\hat{\omega}'\,v(\Delta\mathbf{r}; \hat{\omega}, \hat{\omega}')\rho(\mathbf{r}, \hat{\omega})\rho(\mathbf{r}', \hat{\omega}'), \tag{6}$$

with Ω expressed in units $k_\mathrm{B}T$, $\Delta\mathbf{r} = \mathbf{r}' - \mathbf{r}$, $\mathcal{V}$ the 2D thermal volume of the particle and μ the chemical potential. The functional is known to give accurate results for dense fluids of soft spheres with bounded potentials [20–22]. Recently, it was shown that the approach also works well for fluids of soft anisometric particles [23]. The minimum condition on the functional, $\delta\Omega[\rho]/\delta\rho = 0$, leads to a nonlinear integral equation

$$\ln[\mathcal{V}\rho(\mathbf{r}, \hat{\omega})] + \int \mathrm{d}\mathbf{r}'\,\mathrm{d}\hat{\omega}'\,v(\Delta\mathbf{r}; \hat{\omega}, \hat{\omega}')\rho(\mathbf{r}', \hat{\omega}') = \mu, \tag{7}$$

to be solved for the equilibrium distribution $\rho(\mathbf{r}', \hat{\omega}')$ at a given μ.

3.1. Phase diagram in two dimensions

Let us first focus on localizing the isotropic-to-nematic transition for 2D systems. As the average density in both states is spatially *uniform*, i.e. independent of $\mathbf{r}$, we may write $\rho(\mathbf{r}, \hat{\omega}) = \rho f(\hat{\omega})$, where ρ is the density and f an orientational distribution, subject to the normalization condition $\int \mathrm{d}\hat{\omega}\, f(\hat{\omega}) = 1$. In the isotropic (I) state, all orientations are equally probable and f_{I} is a constant, while in the nematic (N) phase f_{N} is expected to be strongly peaked around the nematic director, which we assume to be spatially uniform. This implies that long-range orientational order is always present in the theory since fluctuations or local defects in the director field are not taken into account. Introducing the angle $\varphi \in [0, \pi]$ between the particle and the nematic director, we may rewrite equation (7) into a self-consistency equation for $f(\varphi)$,

$$f(\varphi) = Z^{-1} \exp\left[-\rho \int \mathrm{d}\varphi'\, E(\varphi, \varphi') f(\varphi')\right], \tag{8}$$

where $Z = \int \mathrm{d}\varphi \exp[\cdots]$ to ensure normalization. Note that $f(\varphi) = f(\pi - \varphi)$ due to the inversion symmetry. The kernel $E(\varphi, \varphi')$ is given by the following spatial integration:

$$E(\varphi, \varphi') = \int \mathrm{d}\Delta\mathbf{r}\, v(\Delta\mathbf{r}; \varphi, \varphi'). \tag{9}$$

The spatial integration in equation (9) can then be carried out without difficulty to give

$$E(\varphi, \varphi') = \epsilon(1 + \nu)\pi a^2 \left(1 - |\cos(\varphi' - \varphi)|^p\right). \tag{10}$$

With this result it is expedient to rewrite equation (8) in the following way:

$$f(\varphi) = Z^{-1} \exp\left[c \int \mathrm{d}\varphi'\, |\cos(\varphi' - \varphi)|^p f(\varphi')\right], \tag{11}$$

where we have introduced the *effective* dimensionless density

$$c = \pi(1 + \nu)\rho a^2 \epsilon. \tag{12}$$

The combination $\rho\epsilon$ in equation (12) illustrates the fact that phase transitions in the *off-lattice* model of equation (3) can be brought about by either increasing the density or lowering the temperature. In contrast, for the *lattice* liquid crystal model of equation (2), phase transitions can be induced via the temperature only [17].

It is clear that the isotropic distribution $f_{\mathrm{I}} = 1/\pi$ is a trivial solution of equation (11) at all densities c. However, at high densities non-trivial, i.e. nematic, solutions are expected to branch off from the isotropic one. To locate the branching point (denoted by $c^\star$) we will perform a simple stability analysis of equation (11), along the lines of [24, 25]. Let us introduce the expansions around the isotropic solution

$$\begin{aligned} f(\varphi) &= \frac{1}{\pi}\left[1 + \alpha a_1 \cos 2\varphi + \alpha^2 a_2 \cos 4\varphi + \cdots\right], \\ c &= c_0 + \alpha c_1 + \alpha^2 c_2 + \cdots, \end{aligned} \tag{13}$$

in terms of a single order parameter α. Likewise, we may expand the kernel as follows:

$$|\cos(\varphi' - \varphi)|^p = \sum_{n \geqslant 0} k_{2n}(p) \cos(2n\varphi) \cos(2n\varphi'), \tag{14}$$

with coefficients

$$k_{2n}(p) = \frac{4}{\pi^2} \int \mathrm{d}\varphi \int \mathrm{d}\varphi'\, |\cos(\varphi' - \varphi)|^p \cos(2n\varphi) \cos(2n\varphi'). \tag{15}$$

Inserting all expansions back into equation (11) and keeping all contributions up to $\mathcal{O}(\alpha)$ gives the branching or bifurcation point

$$c^\star = c_0 = 2/k_2(p), \tag{16}$$

implying that stable nematic solutions are expected for $c > c^\star$. We remark that for $p = 1$ the branching density $c^\star = 3\pi/2$ is identical to that of the 2D Onsager theory for infinitely thin hard needles [18]. This can be shown by replacing $|\cos(\varphi' - \varphi)|$ in equation (15) by the Onsager kernel $-|\sin(\varphi' - \varphi)|$, see [18]. Both kernels yield the same coefficient $k_2 = 4/(3\pi)$, and hence the same bifurcation density $c^\star = 3\pi/2$.

To verify the thermodynamic stability of the nematic solutions close to the branching density we must analyse its free energy. The dimensionless Helmholtz free energy (ignoring all irrelevant constants) is given by

$$F[f]/N \sim \langle \ln[c\pi f(\varphi)] \rangle + \frac{c}{2} \langle\langle (1 - |\cos(\varphi' - \varphi)|^p) \rangle\rangle, \tag{17}$$

where $\langle \cdots \rangle = \int \mathrm{d}\varphi \, f(\varphi)$. The free-energy difference $\Delta F = F_\mathrm{N} - F_\mathrm{I}$ between the nematic and isotropic states close to the branching point can be written in Landau form in terms of the nematic order parameter α

$$\Delta F/N = A\alpha^2 + B\alpha^3 + C\alpha^4. \tag{18}$$

The coefficients can be obtained from extending the bifurcation analysis to higher order in α (using the expansions equations (13) and (14)) and performing an order-by-order solution of equation (11) up to $\mathcal{O}(\alpha^3)$. The algebra is straightforward but tedious and we will only give the final outcome here. It turns out that $A, B = 0$ while

$$C = -\frac{k_2(p) - 2k_4(p)}{64[k_2(p) - k_4(p)]}. \tag{19}$$

The sign of C provides a hallmark for the order of the transition. If it is negative, nematic perturbations around the branching point lower the free energy of the system and the transition is expected to be continuous. If C is positive the incipient free-energy difference goes up for small α, which means that the actual phase transition involves a density jump and is first order. In the latter case the coexisting densities are indicated by binodal curves, which can be computed in the usual way by requiring the pressure and chemical potential to be equal in the coexisting phases. The equilibrium $f(\varphi)$ for a given nematic density c is obtained numerically from the consistency equation (11) by dividing the interval $[0, \pi/2]$ into 100 equidistant grid points and employing the iteration scheme outlined in [26].

Figure 1 shows that the isotropic–nematic transition is continuous for small p but becomes first order for $p > 8$. The full phase diagram in figure 2 shows that the actual cross-over from continuous to first order (marked by the tri-critical point where all phase lines meet) is located at a somewhat lower value for p, namely $p = 4.7$. The discrepancy is expected since the bifurcation analysis usually provides an *upper* estimate for the critical points. We also remark that the non-monotonic behaviour of the critical density at low p is consistent with the simulation results of the generalized LL model reported in [17]. The steep increase of the nematic order parameter in figure 3 suggests that a considerable degree of nematic order is expected in the coexisting nematic phase at large p.

3.2. Asymptotic results for large p

For very large p (say larger than 100) the solution of equation (11) on a grid becomes numerically awkward since $f(\varphi)$ becomes extremely peaked at $\varphi = 0$ (and π). It is therefore tempting to formulate a simple variational theory that allows us to access the phase diagram at

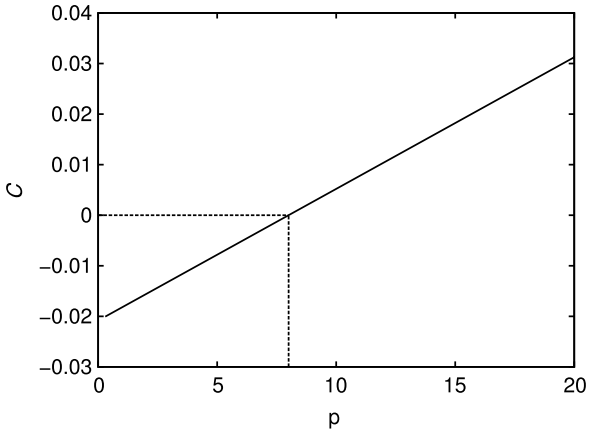

Figure 1. Landau coefficient C (equation (19)) versus p. For $p > 8$ the isotropic–nematic transition is first order; for smaller p it is continuous.

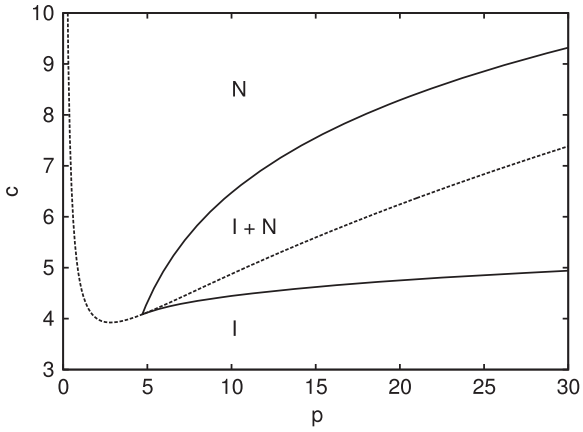

Figure 2. Theoretical phase diagram. Plotted is the dimensionless concentration c versus p. The dashed curve represents the nematic branching line $c^\star$, calculated from equation (16). The binodals are given by the solid curves. A tri-critical point is located at $p = 4.7$.

asymptotically large p. Indeed, for highly nematic states $f(\varphi)$ is well described by a Gaussian trial function with variational parameter $\beta \gg 1$ [27],

$$f(\varphi) \sim \left(\frac{2\beta}{\pi}\right)^{1/2} \exp\left[-\frac{1}{2}\beta\varphi^2\right], \qquad \text{for } 0 \leqslant \varphi \leqslant \frac{\pi}{2}, \tag{20}$$

and its mirrored version $f(\pi - \varphi)$ for the interval $\pi/2 \leqslant \varphi \leqslant \pi$. Inserting the Gaussian into equation (17) and integrating yields the following asymptotic result for the ideal free energy (first term):

$$\begin{aligned} \langle \ln[c\pi f(\varphi)] \rangle &\sim \ln c + \tfrac{1}{2}\ln 2\pi\beta - \tfrac{1}{2} \qquad \text{(N)}, \\ &= \ln c \qquad\qquad\qquad\quad \text{(I)}, \end{aligned} \tag{21}$$

valid for large β. Using the approximation

$$|\cos x|^p \approx \exp[-(1/2)px^2] \qquad (p \gg 1), \tag{22}$$

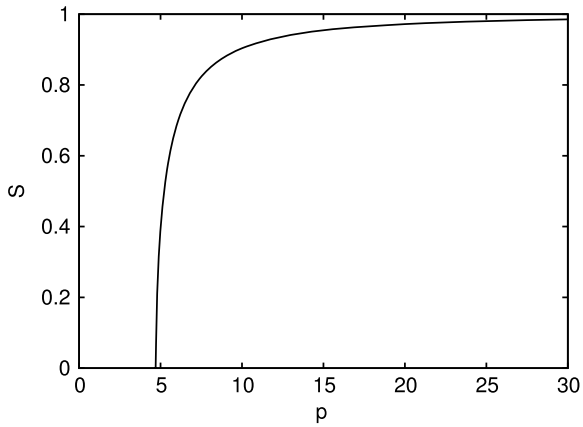

Figure 3. Nematic order parameter $S = \langle \cos 2\varphi \rangle$ corresponding to the nematic binodal in figure 2.

in the excess free energy (second term) allows us to calculate the double orientational averages analytically

$$\langle\langle |\cos(\varphi' - \varphi)|^p \rangle\rangle \sim \left(\frac{\beta}{\beta + 2p}\right)^{1/2} \quad \text{(N)},$$
$$\sim \left(\frac{2}{\pi p}\right)^{1/2} \quad \text{(I)}. \tag{23}$$

The value of β is fixed (at a given density) by minimizing the total nematic free energy with respect to the variational parameter. Some rearranging then leads to the following minimization condition:

$$\left(\frac{\beta}{p} + 2\right)^3 - c^2 \frac{\beta}{p} = 0, \tag{24}$$

which has to be solved numerically along with the coexistence equations for the chemical potential and pressure at a given p. These follow straightforwardly from the free-energy equation (17). The resulting binodals and coexistence chemical potential are shown in figures 4 and 5, respectively.

Finally, we want to point out that the bifurcation density $c^\star$ at large p scales as $c^\star \propto p^{1/2}$. The scaling relation can be easily established by making an asymptotic expansion of k_2 from equation (15). For the regime $p \gg 1$ one can show with the aid of equation (22) that

$$k_2(p) \propto \int_0^\infty \mathrm{d}(\varphi' - \varphi)\, \exp[-(1/2)\, p(\varphi' - \varphi)^2],$$
$$\propto p^{-1/2}, \tag{25}$$

up to leading order, hence $c^\star \propto p^{1/2}$. This result is analogous to the scaling of the critical coupling constant in the LL simulations of [17].

3.3. Isotropic–nematic interface

To assess the properties of the interface between the coexisting isotropic and nematic phases we have to go back to our initial DFT formulation in section 3. If we assume the interface to be flat with a surface normal $\hat{x}$, the one-particle density will be non-uniform along this direction

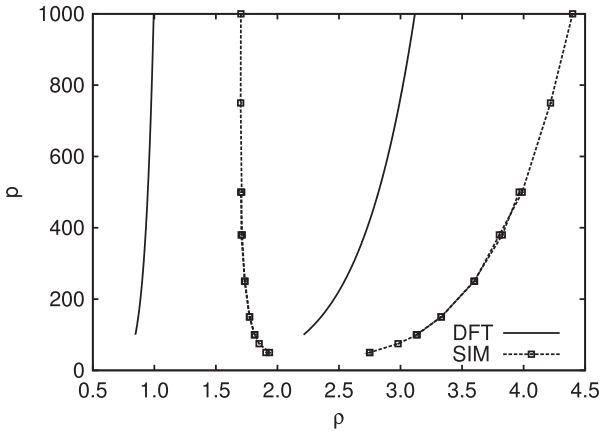

Figure 4. Phase diagram of the two-dimensional liquid crystal model of equation (3) using $\epsilon = 2.5$. The solid curves show the theoretical binodals, obtained using the large p approximation. Plotted is the dimensionless density $\rho = Na^2/A$ of the isotropic phase (left curve) and the nematic phase (right) versus p. Also shown are the corresponding simulation results (squares), where the dashed lines serve to guide the eye.

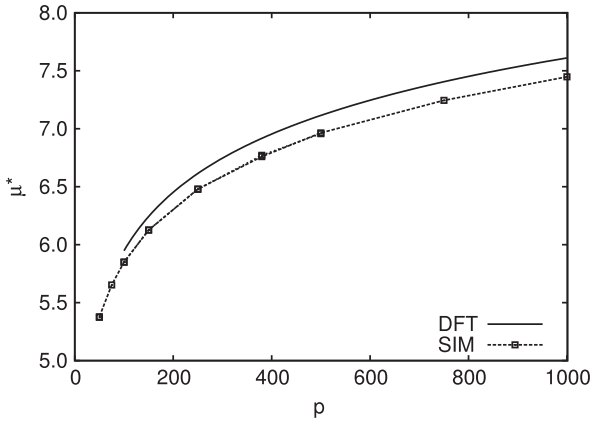

Figure 5. Coexistence chemical potential $\mu^\star$ versus p corresponding to figure 4. The solid curve is the theoretical result; squares are simulation results.

and depend on the spatial coordinate $x = \mathbf{r} \cdot \hat{x}$ and angle φ. It is a solution of the integral equation (7) with $\mu = \mu^\star$,

$$\ln[\mathcal{V}\rho(x,\varphi)] + \int \mathrm{d}x'\,\mathrm{d}\varphi'\, E_x(\Delta x;\varphi,\varphi';\vartheta)\rho(x',\varphi') = \mu^\star, \tag{26}$$

$\mu^\star$ being the chemical potential at coexistence, $\Delta x = x' - x$, subject to the boundary conditions

$$\rho(x,\varphi) = \begin{cases} \rho_{\mathrm{I}} f_{\mathrm{I}}, & (x \to -\infty), \\ \rho_{\mathrm{N}} f_{\mathrm{N}}(\varphi), & (x \to \infty), \end{cases} \tag{27}$$

(recall that $\varphi = \arccos(\hat{n} \cdot \hat{w})$). In equation (26), the kernel E_x is defined as the pair potential (at fixed orientations) averaged over the distance Δy perpendicular to $\hat{x}$ along which the system

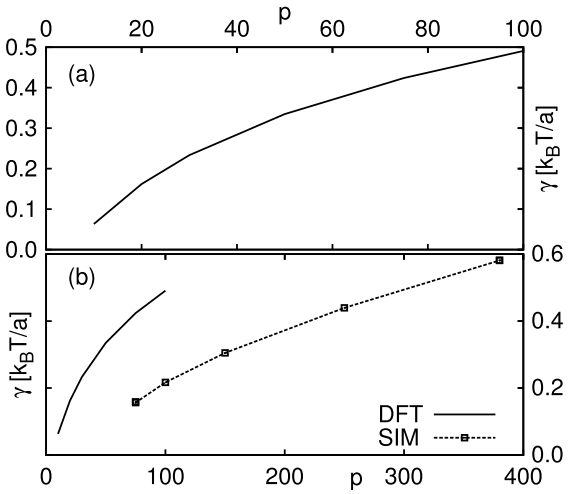

Figure 6. Line tension γ (in units $k_{\rm B}T/a$) for $\epsilon = 2.5$ versus p. (a) DFT result. (b) Computer simulation results (squares), together with the DFT result (solid curve) for comparison. Note the different p-range in the above plots.

is homogeneous

$$E_x(\Delta x; \varphi, \varphi'; \vartheta) = \int_{-\infty}^{\infty} {\rm d}\Delta\, y v(\Delta \mathbf{r}; \varphi, \varphi'; \vartheta). \tag{28}$$

Note that because of the broken spatial symmetry the integral depends implicitly on the *anchoring angle* $\vartheta = \arccos(\hat{n} \cdot \hat{x})$ between the nematic director $\hat{n}$ and the surface normal. This becomes manifest when we focus on the translation–rotation coupling contribution σ in equation (4). In explicit form it reads

$$\sigma = 1 + \nu \left[(\Delta \hat{\mathbf{r}} \cdot \mathcal{R}_\vartheta \hat{\omega})^2 + (\Delta \hat{\mathbf{r}} \cdot \mathcal{R}_\vartheta \hat{\omega}')^2 \right], \tag{29}$$

with $\Delta \hat{\mathbf{r}} = \{\Delta x, \Delta y\}/(\Delta x^2 + \Delta y^2)^{1/2}$ the centre-of-mass difference unit vector, $\hat{\omega} = \{\cos\varphi, \sin\varphi\}$ and $\mathcal{R}_\vartheta$ the rotation matrix

$$\mathcal{R}_\vartheta = \begin{pmatrix} \cos\vartheta & -\sin\vartheta \\ \sin\vartheta & \cos\vartheta \end{pmatrix}. \tag{30}$$

Clearly, if $\nu = 0$ there is no dependence on ϑ and the interfacial profiles are *identical* for all anchoring angles. The ϑ-dependence also vanishes for the bulk case, as it should. This can easily be verified by carrying out the total spatial integral of σ (cf equation (9)). However, if $\nu \neq 0$, the translational and rotational degrees of freedom are coupled and the interfacial properties will in general be dependent upon the anchoring angle. In particular, we are interested in the line tension γ which can be extracted from the equilibrium interfacial density profile. Inserting the one-body density into the functional equation (7) yields the minimum grand potential

$$\Omega_{\rm min} = \int {\rm d}\mathbf{r} \int {\rm d}\varphi\, \rho(\mathbf{r}, \varphi) \left\{ \tfrac{1}{2} \ln[\mathcal{V}\rho(\mathbf{r}, \varphi)] - 1 - \tfrac{1}{2}\mu^\star \right\}. \tag{31}$$

The line tension $\gamma[\mu^\star(p), \nu, \vartheta]$ is then obtained from the standard thermodynamic relation $\gamma = (\Omega_{\rm min} + PA)/L$, with P the coexistence pressure.

In figure 6 we show the line tension for $\nu = 0$. To facilitate comparison with simulations later on we will henceforth fix the coupling parameter to $\epsilon = 2.5$. Note that, owing to

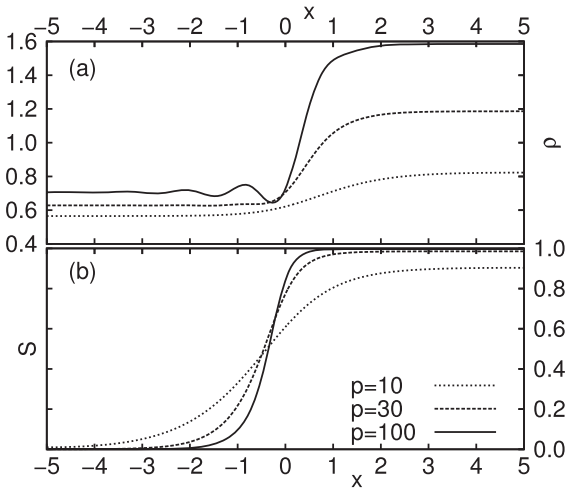

Figure 7. Interfacial profiles for (a) the density $\rho(x)$ and (b) the nematic order parameter $S(x)$ for $\nu = 0$.

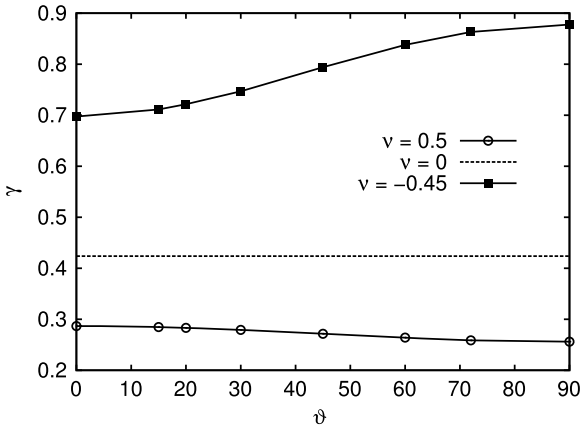

Figure 8. Line tension γ (in units $k_B T/a$) versus anchoring angle ϑ (in degrees), for several values of ν as indicated.

equation (12), changing this value does not give qualitatively different results but merely constitutes a linear shift in γ and ρ. The increase of γ as a function of p reflects the transition becoming strongly first order at large p. The corresponding interfacial profiles for the density $\rho(x)$ and the nematic order parameter $S(x)$, defined as

$$\begin{aligned} \rho(x) &= \int \mathrm{d}\varphi\, \rho(x,\varphi), \\ S(x) &= \rho^{-1}(x) \int \mathrm{d}\varphi\, \rho(x,\varphi) \cos 2\varphi, \end{aligned} \tag{32}$$

are shown in figure 7. As expected, the interface becomes sharper for large p. For $p = 100$ small density oscillations on the isotropic side occur, which point to a layering effect induced by the interface.

Let us now focus on the anchoring behaviour for a fixed value of $p = 75$ and $\nu \neq 0$. The results, summarized in figure 8, show a strong dependency of the line tension on the anchoring

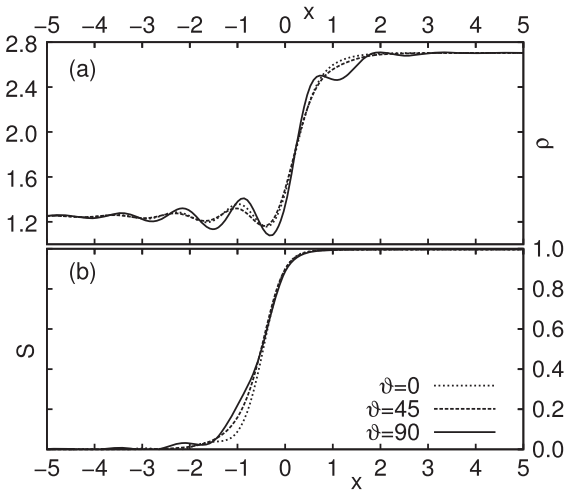

Figure 9. Interfacial profiles for $p = 75$, $\nu = -0.45$ at different anchoring angles ϑ (in degrees).

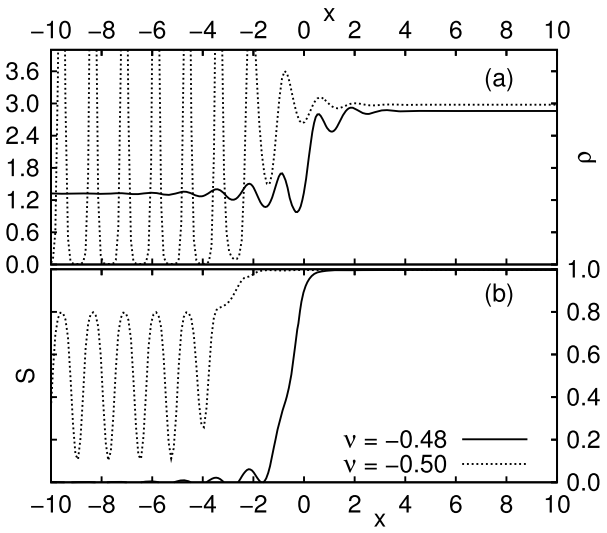

Figure 10. Interfacial profiles for $p = 75$ and anchoring angle $\vartheta = 90°$.

angle ϑ, especially for $\nu < 0$. Recall that end-to-end pair configurations are energetically more favourable than side-to-side ones in this case. While for $\nu < 0$ the minimal tension is at $\vartheta = 0$ implying *perpendicular* surface anchoring, a positive ν seems to be associated with *parallel* anchoring. Investigations for other p reveal that this phenomenon is robust. Microscopic information extracted from the profiles for $\nu = -0.45$ is given in figure 9. These reveal that the layering effect is considerably influenced by the anchoring angle. In particular, particles show enhanced localization across the interface if the nematic director is forced to be parallel to the interface.

An even more dramatic effect is encountered if we lower $\nu \to -0.5$; see figure 10. Note that, for $\nu = -0.5$, the end-to-end configurations have zero repulsion and are therefore strongly favoured. This explains the tendency of the system to form string-like clusters along

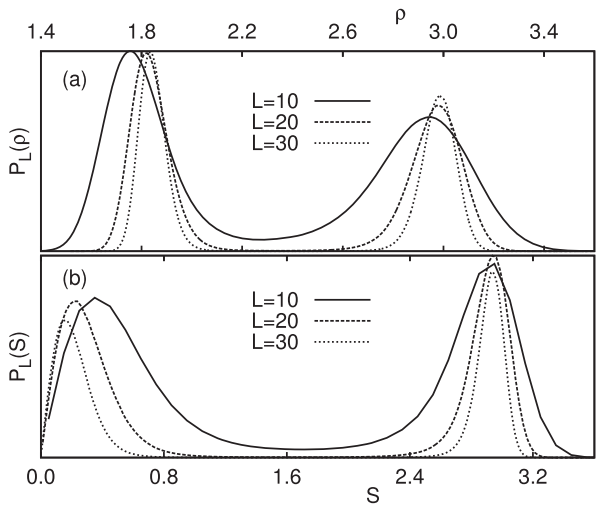

Figure 11. (a) Coexistence distributions $P_L(\rho, \mu)$ for various system sizes L as indicated, with $\rho = Na^2/A$ the dimensionless particle density. The coexistence between the two phases is manifested by 'equal area' under the peaks. (b) The corresponding distributions $P_L(S)$ of the nematic order parameter S, given by equation (34).

the interface as indicated by the sharp density peaks in figure 10. However, $\nu = -0.5$ seems to be a rather pathological case. The density modulations penetrate deeply into the isotropic phase, which raises strong suspicions as to whether the isotropic fluid state is stable against clustering or crystallization. It remains to be checked by simulations whether the IN transition is really pre-empted by a freezing transition in this case.

4. Computer simulation

Next, we will confirm some of the theoretical results using computer simulation. To this end, grand canonical (GC) Monte Carlo simulations [28, 29] are performed, at chemical potential μ, for the model of equation (3) using $\epsilon = 2.5$. Again, for the radial part, we take the step function of equation (5). In this work, we restrict the simulations to the case $\nu = 0$ in equation (3). A computer simulation study of anchoring effects, predicted by the theory to occur when $\nu \neq 0$, will be postponed to a future publication.

4.1. Finite-size scaling results for $p = 75$

We begin the simulations using $p = 75$ in equation (3). Inspired by our theoretical results, we expect that, for $p = 75$, a first-order phase transition should occur, when the chemical potential is tuned to its coexistence value $\mu^\star$. In GC simulations, $\mu^\star$ is determined from the distribution $P_L(\rho, \mu)$, defined as the probability to observe a particle density ρ in the system. In order to also simulate the regions of low probability, a biased sampling scheme is implemented [30, 31]. The distribution $P_L(\rho, \mu)$ depends on the chemical potential μ, as well as on the size of the $L \times L$ simulation square (periodic boundary conditions are assumed). At $\mu = \mu^\star$, $P_L(\rho, \mu)$ becomes bimodal, with two peaks of equal area. In computer simulations, the transition can thus be located by varying μ until the 'equal-area' criterion is obeyed.

Indeed, we find that bimodal density distributions can be realized in this way. Figure 11(a) gives some examples for various system sizes L. By increasing L, the peaks become more

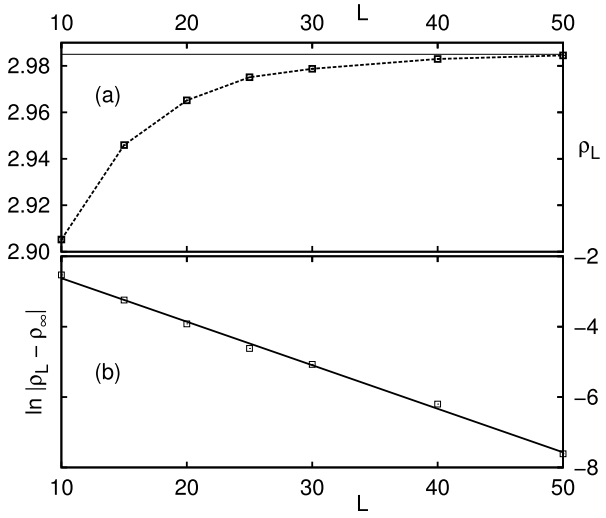

Figure 12. Finite-size scaling of the position of the high-density peak in $P_L(\rho, \mu)$ of figure 11(a). (a) Peak position ρ_L as a function of L. The horizontal line marks the density ρ_∞ in the thermodynamic limit. (b) Finite-size scaling analysis using equation (33). The straight line is a linear fit; see the details in the text.

narrow. This is to be expected because, in the thermodynamic limit $L \to \infty$, one has a sharp transition, and, consequently, a distribution featuring two δ-peaks. In addition, closer inspection of figure 11(a) also reveals a finite-size effect in the peak *positions*. Finite-size effects at first-order phase transitions have received considerable attention [32–34]. We believe that the current state-of-the-art in this field is the rigorous treatment of Borgs and Kotecky [34]. More precisely, for two-phase coexistence data obtained using the 'equal-area' rule, an exponential L-dependence is predicted

$$R \equiv |X_L - X_\infty| \leqslant \mathcal{O}(\mathrm{e}^{-\tau L}). \tag{33}$$

Here, X_L is the property of interest as obtained in the finite system of size L, X_∞ the corresponding value in the thermodynamic limit, and τ a constant.

In figure 12(a), we show the position ρ_L of the high-density (nematic) peak of $P_L(\rho, \mu)$ as a function of L. Next, we use equation (33) to estimate the density ρ_∞ of the nematic phase in the thermodynamic limit. To this end we have plotted, in figure 12(b), the logarithm of R as a function of system size L. Here, ρ_∞ was taken to be a fit parameter, and tuned until the graph of $\ln R$ versus L became linear. For $\rho_\infty \approx 2.985$, we find that $\ln R$ indeed becomes linear in L, which thus serves as our best estimate of the nematic density in the thermodynamic limit. For completeness, this estimate has also been marked in figure 12(a) as the horizontal line. The density of the low-density (isotropic) peak can be obtained analogously. The corresponding scaling plot is qualitatively similar to figure 12 and therefore not shown here. For the density of the isotropic phase in the thermodynamic limit, we obtain $\rho_\infty \approx 1.850$.

In addition, we also observe an L-dependence in the coexistence chemical potential $\mu_L^\star$. Recall that $\mu_L^\star$ corresponds to the chemical potential at which 'equal area' in $P_L(\rho, \mu)$ of the *finite* system is observed. Shown in figure 13(a) is $\mu_L^\star$ versus L. Again, Borgs and Kotecky predict an exponential L-dependence given by equation (33). We may therefore estimate $\mu_\infty^\star$ as before, by plotting $\ln R$ versus L, using for $\mu_\infty^\star$ that value at which the data become linear. The result is shown in figure 13(b). Again, the data follow the straight line quite well, and we conclude $\mu_\infty^\star \approx 5.6536$.

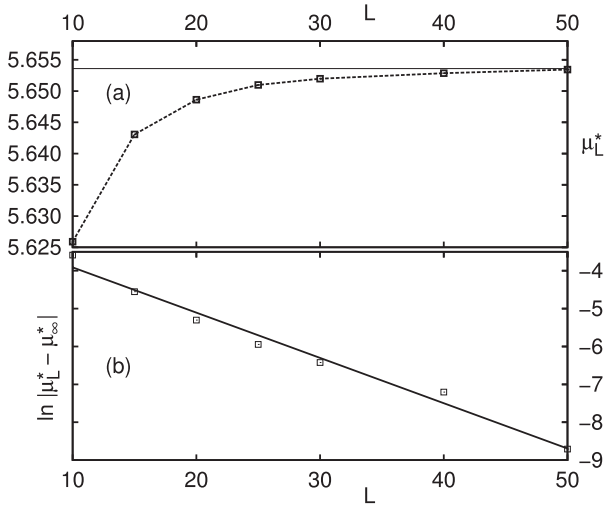

Figure 13. Finite-size scaling of the coexistence chemical potential. (a) $\mu_L^\star$ as a function of L. The horizontal line marks the coexistence chemical potential $\mu_\infty^\star$ in the thermodynamic limit. (b) Finite-size scaling analysis using equation (33). The straight line is a linear fit; see the details in the text.

It is also of interest to consider the distribution $P_L(S)$ at coexistence, with S the nematic order parameter. Here, we define S as the maximum eigenvalue of the orientational tensor

$$Q_{\alpha\beta} = \frac{1}{A}\sum_{i=1}^{N}(2d_{i\alpha}d_{i\beta} - \delta_{\alpha\beta}), \tag{34}$$

with $d_{i\alpha}$ the α component ($\alpha = x, y$) of the orientation $\hat{\omega}_i$ of molecule i, $\delta_{\alpha\beta}$ the Kronecker delta, N the number of particles, and system area $A = L^2$. For an isotropic phase, in the thermodynamic limit, S equals zero. For a 'true' nematic phase, i.e. with long-range order, one has $S > 0$ in the thermodynamic limit. Note that we have normalized equation (34) with the system area A, and not with N as is usually done. The reason to normalize with respect to A is that, in the GC ensemble, N is a fluctuating quantity. Note also that, for a perfectly aligned phase, S becomes identical to the particle density N/A.

Several distributions $P_L(S)$ are shown in figure 11(b). We emphasize that all these distributions were obtained using that value of μ at which 'equal area' in $P_L(\rho, \mu)$ was obtained. The data of figure 11(b) are quite stunning. On the one hand, we observe a pronounced shift of the lower peak toward $S \to 0$. This is to be expected, since this peak corresponds to the isotropic phase. Note that the L-dependence of the isotropic peak does not reveal any physical information: an ideal gas of rods would reveal the same effect. The L-dependence of S in the isotropic phase is purely a numerical artifact. It stems from the fact that S is positive, since the *maximum* eigenvalue of the orientational tensor is always taken. Consequently, the distribution of S in the isotropic phase *cannot* be Gaussian around $S = 0$. Instead, the distribution is 'skewed', with the peak *always* being located at $S > 0$. As the system size is increased, the isotropic peak shifts to zero (see the discussion by Eppenga and Frenkel [35]), precisely what we observe.

In contrast, on the scale of figure 11(b), the nematic peak appears to be rather insensitive to the system size L. In fact, finite-size scaling of the nematic peak position suggests that a finite value S_∞ in the thermodynamic limit is maintained; see figure 14. Shown in figure 14(a) is the

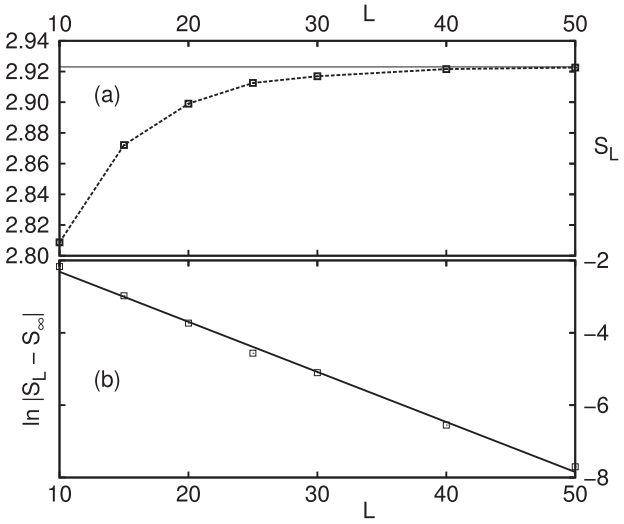

Figure 14. Finite-size scaling of the position of the nematic peak in $P_L(S)$ of figure 11(b). (a) Peak position S_L as a function of L. The horizontal line marks the nematic order parameter S_∞ in the thermodynamic limit. (b) Finite-size scaling analysis using equation (33). The straight line is a linear fit; see the details in the text.

nematic peak position S_L as a function of L. The data are quite interesting, because they show an *increase* of nematic order with increasing system size L. Shown in figure 14(b) is the result of the finite-size scaling analysis using equation (33). Again, S_∞ was obtained by tuning, until the best collapse of the data onto a straight line occurred. For the nematic order parameter in the thermodynamic limit, we obtain $S_\infty \approx 2.923$. Note that, for $\nu = 0$, the liquid crystal potential of equation (3) is separable. For this special case, Straley has proved the *absence* of long-range nematic order in the thermodynamic limit [18]. In other words, S_∞ should become zero, while our finite-size analysis, in contrast, suggests that S_∞ remains finite. For the XY-model in two dimensions, it has been shown that the decay of magnetic order with system size is so slow that one would need a sample 'the size of Texas' [36] to see it. The most likely explanation is therefore that something similar also takes place in our liquid crystal model, and that the data of figure 14(a) will eventually 'turn over' and decay to zero.

Next, we consider the logarithm of the distributions, which essentially reflect *minus* the free energy of the system. Shown in figure 15 is $\ln P_L(S)$ for several system sizes L. Again, we emphasize that the distributions were obtained using that value of μ at which 'equal area' in $P_L(\rho, \mu)$ was obtained. For each distribution $\ln P_L(S)$, we may read off the average peak height ΔF, measured with respect to the minimum between the peaks. By increasing the size of the system, ΔF increases as well. As was shown by Binder, ΔF corresponds to the free-energy cost of having two interfaces in the system [37]. More precisely, in two dimensions, we expect that

$$\Delta F = 2\gamma L, \tag{35}$$

with γ the line tension (the factor of two stems from the use of periodic boundary conditions, which lead to the formation of two interfaces in the system; see also the snapshot of figure 17). Shown in figure 16(a) is ΔF as a function of L; the data are indeed well described by a straight line through the origin. From the slope of the line, we obtain $\gamma = 0.158\, k_B T/a$. Of course, we may also read off the barrier in $\ln P_L(\rho, \mu)$, shown in figure 16(b). Again, a linear increase

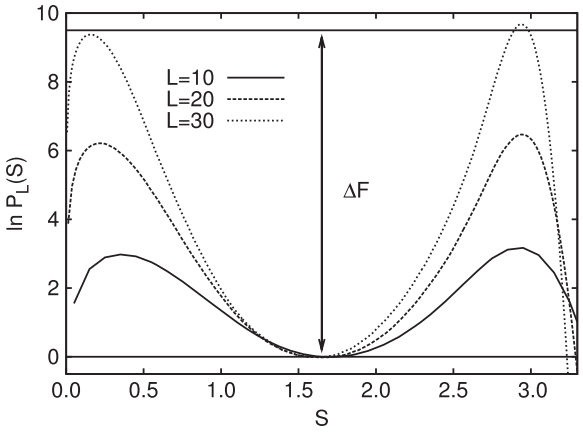

Figure 15. Distributions $\ln P_L(S)$ for various system sizes L as indicated. Also marked is ΔF for the $L = 30$ system.

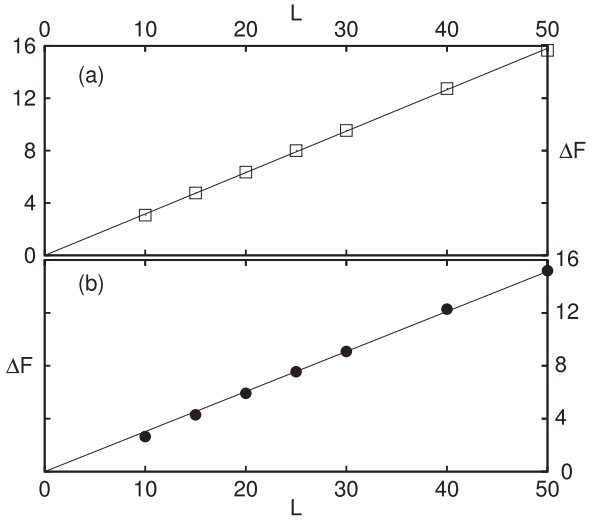

Figure 16. (a) Free-energy barrier ΔF, extracted from the distributions $\ln P_L(S)$ of figure 15, as a function of L. The straight line is a fit to equation (35). (b) The same as (a), but with ΔF extracted from $\ln P_L(\rho, \mu)$.

of ΔF is observed, and from the slope of the line we obtain $\gamma = 0.151\, k_B T/a$, which is very close to our previous estimate.

In summary, and in agreement with our theoretical results, we find that an exponent $p = 75$ is high enough to induce a first-order transition in the *off-lattice* liquid crystal model of equation (3). The scaling of the coexisting densities with system size is well described by what is expected for such a transition. The same also holds for the growth of the free-energy barrier ΔF. An interesting and unexpected result, which certainly requires further elaboration, is the scaling of the nematic order parameter; see figure 14. If the trend continues for $L \to \infty$, long-range nematic order in a two-dimensional liquid crystal would, after all, be possible.

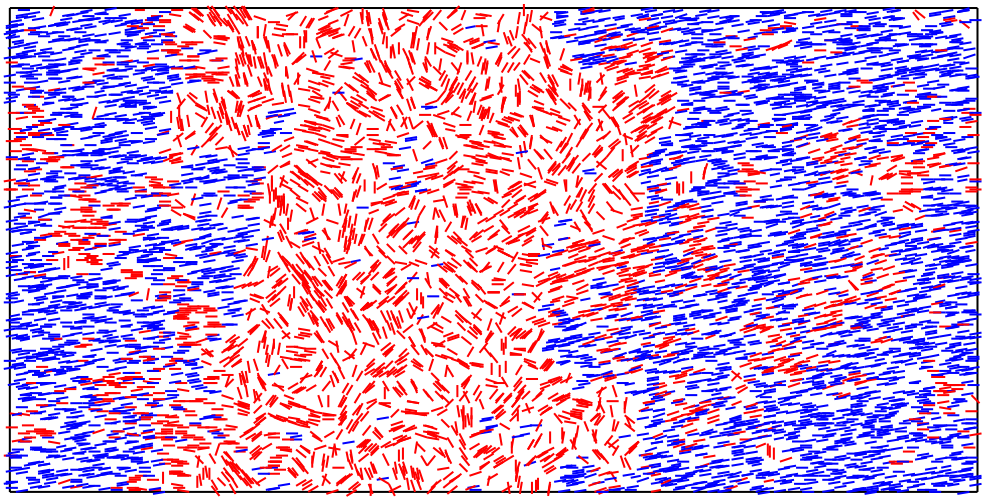

Figure 17. Simulation snapshot obtained in the coexistence region for $p = 60$. Each line segment represents a particle. Clearly visible is that the system has phase-separated into an isotropic domain and a nematic domain (where we leave open the question whether the nematic phase exhibits true long-range order or only quasi-long-range order). Note also that the interfaces are not flat, and that they appear to be decorated with capillary waves.

(This figure is in colour only in the electronic version)

4.2. Results for different p

We have also measured the coexistence densities, chemical potential, and line tension for different values of p, while keeping $\nu = 0$ and $\epsilon = 2.5$. Here, we did not perform a detailed finite-size scaling analysis. Instead, the data for $p \neq 75$ were obtained in a single simulation of a (reasonably large) system. In figure 4, we show the density of the isotropic phase, and of the nematic phase, as a function of p. Note that the region in between the curves corresponds to phase coexistence. If one performs a simulation in this region, for example by keeping the density fixed, snapshots strikingly reveal the two-phase coexistence; see figure 17. Shown in figure 5 is the coexistence chemical potential $\mu^\star$ versus p, compared to the DFT result. Finally, in figure 6(b), we show the line tension versus p.

5. Discussion and summary

In summary, we have provided strong evidence that *off-lattice* liquid crystals in two dimensions can also undergo first-order phase transitions. To this end, the pair potential of equation (3) was introduced, constructed to be purely repulsive and short ranged and to obey inversion symmetry. The first-order transition takes place when the pair potential becomes sufficiently 'sharp and narrow', i.e. for a sufficiently large exponent p in equation (3). A simple DFT calculation puts the threshold value at around $p = 8$. When $p > 8$, the theory predicts a first-order transition from a low-density (isotropic) phase to a high-density (nematic) phase. In other words, there is a finite density gap between the two phases, as well as a jump in the nematic order parameter.

An important conclusion of this work is that many of the trends predicted by the theory also appear in the computer simulations. In other words, key properties of equation (3) are already captured at the mean-field level. This finding is somewhat surprising because, in low spatial dimension, mean field is typically assumed to be unreliable. The simulations, in agreement

with the theory, find strong evidence of a first-order transition, already at $p > 50$. Note that we have backed our simulations with a detailed investigation of finite-size effects, and that these were shown to be consistent with a first-order phase transition. We have not determined in our simulations the precise value of p where the cross-over from continuous to first order occurs, since such simulations would be extremely time consuming, but we expect this will exceed the theoretical bound $p = 8$ significantly.

Nevertheless, for those values of p where the simulations do observe the first-order transition, a profound density gap between the two coexisting phases is found; see the phase diagram of figure 4. In the limit of large p, theory and simulation are in qualitative agreement: both show an increase in density of the nematic phase with p, while the density of the isotropic phase is much less sensitive to p. At lower p, qualitative discrepancies arise, but these can be attributed to the large-p approximation used by the theory, which obviously breaks down here. Interestingly, when comparing the coexistence chemical potential $\mu^\star$ between theory and simulation (see figure 5) the agreement is remarkably good, also at low p. Apparently, the breaking down of the large p approximation does not affect $\mu^\star$ as much as it does the coexistence densities. With regards to the line tension (see figure 6), the agreement between theory and simulation is merely qualitative: by increasing p, the tension increases in both cases, but the actual numerical values differ profoundly. A possible explanation may be the presence of capillary-wave interface fluctuations. These fluctuations are neglected in the theory, while the simulation snapshot of figure 17 suggests that interface fluctuations are actually quite strong.

A rather controversial result of this work is the value of the nematic order parameter S in the nematic phase. The DFT result (see figure 3) predicts rather large values of S, once the transition has become first order. Of course, in realistic systems, one always has defects, which are expected to destroy nematic order in the thermodynamic limit. Since such defects are discarded by the theory, we expect that figure 3 is merely an artifact, and that realistic systems in the thermodynamic limit will always have $S = 0$, regardless of the value of p. Still, it is somewhat surprising that our computer simulations also suggest that $S > 0$, see figure 14, and that the finite size effects in our data are *not* compatible with a decay of S to zero. At this point, the most likely explanation is that the decay of S with system size only shows up in macroscopically large samples, which are clearly out of reach in any foreseeable simulation.

Note that our theory has also made a number of intriguing predictions for the case where the translational and orientational degrees of freedom are coupled, i.e. when $\nu \neq 0$. In this case, strong anchoring effects are predicted, as well as the possibility of the isotropic-to-nematic transition being pre-empted by freezing. Since our particles are ultra-soft, the formation of stable aggregate or cluster mesophases as encountered in various soft sphere systems [38, 39] is also possible. All these scenarios need to be verified by computer simulation. We are currently developing new simulation methodology to study anchoring effects at the isotropic–nematic interface; some preliminary information about the method is already available [40]. The application of these new techniques to the 2D liquid crystal model of the present work is therefore postponed to a future publication.

Of course, it would be interesting if some of our findings could be confirmed in experiments. As we had already remarked in the introduction, the condition of phase coexistence is obtained straightforwardly by keeping the density fixed at some value in the coexistence region. The problem will most likely be to achieve sufficiently 'sharp and narrow' interactions. One possibility that we envision is to use a mixture of colloidal rods and non-adsorbing polymers. Despite the fact that colloidal rods cannot overlap, unlike the particles considered here, and that the addition of polymer renders the *effective* rod interactions *attractive*, which may induce an additional gas–liquid phase separation, we believe a first-order isotropic–nematic phase transition could be feasible. In particular, looking at the phase

diagrams reported for 3D rod–polymer mixtures [41] we anticipate that the strong polymer-induced widening of the isotropic–nematic coexistence region carries over to 2D systems as well, and might induce a first-order transition. A prerequisite for this scenario is that both the size ratio (of rod length to polymer radius of gyration) and the polymer concentration are sufficiently large.

Finally, we would like to remind the reader that the original idea of this work, namely to use 'sharp and narrow' interactions, is not new, and goes back to the work of [11]. Here, the approximate correspondence between generalized XY-models and the Potts model [42] was already exploited to demonstrate the possibility of having a first-order transition in a 2D spin system with continuous degrees of freedom. The extension of this work has been to apply the same ideas to *off-lattice* liquid crystals. Nevertheless, the approximate link to the Potts model can still be uncovered, using $q \propto p^{1/2}$ [12]. Here, p is the exponent in equation (3), and q the number of Potts states. Note that this relation is valid only asymptotically for large p. Many of the results of this work, for example the cross-over from a continuous to a first-order transition (figure 1), the variation of $\mu^\star$ with p (figure 5), and even the increase of the line tension with p (figure 6), have their analogues in the 2D Potts model (see for example [43], where an explicit formula for the line tension of the Potts model is given).

Acknowledgment

This work was supported by the *Deutsche Forschungsgemeinschaft* under the SFB-TR6 (project section D3).

References

[1] Kosterlitz J M 1974 *J. Phys. C: Solid State Phys.* **7** 1046
[2] Lebwohl P A and Lasher G 1972 *Phys. Rev.* A **6** 426
[3] Mermin N D and Wagner H 1966 *Phys. Rev. Lett.* **17** 1133
[4] Frenkel D and Eppenga R 1985 *Phys. Rev.* A **31** 1776
[5] Bates M A and Frenkel D 2000 *J. Chem. Phys.* **112** 10034
[6] Lagomarsino M C, Dogterom M and Dijkstra M 2003 *J. Chem. Phys.* **119** 3535
[7] Kosterlitz J M and Thouless D J 1972 *J. Phys. C: Solid State Phys.* **5** L124
[8] Kosterlitz J M and Thouless D J 1973 *J. Phys. C: Solid State Phys.* **6** 1181
[9] Farinas-Sanchez A I, Paredes R and Berche B 2005 *Phys. Rev.* E **72** 031711
[10] Berche B and Paredes R 2005 *Condens. Matter Phys.* **8** 723
[11] Domany E, Schick M and Swendsen R H 1984 *Phys. Rev. Lett.* **52** 1535
[12] Blöte H W J, Guo W and Hilhorst H J 2002 *Phys. Rev. Lett.* **88** 047203
[13] Jonsson A, Minnhagen P and Nylén M 1993 *Phys. Rev. Lett.* **70** 1327
[14] van Enter A C D, Romano S and Zagrebnov V A 2006 *J. Phys. A: Math. Gen.* **39** L439
[15] van Enter A C D and Shlosman S B 2005 *Commun. Math. Phys.* **255** 21
[16] van Enter A C D and Shlosman S B 2002 *Phys. Rev. Lett.* **89** 285702
[17] Vink R L C 2007 *Phys. Rev. Lett.* **98** 217801
[18] Straley J P 1971 *Phys. Rev.* A **4** 675
[19] Evans R 1979 *Adv. Phys.* **28** 143
[20] Grewe N and Klein W 1977 *J. Math. Phys.* **64** 1729
[21] Lang A, Likos C N, Watzlawek M and Löwen H 2000 *J. Phys.: Condens. Matter* **12** 5087
[22] Archer A J 2005 *J. Phys.: Condens. Matter* **17** 1405
[23] Rex M, Wensink H H and Löwen H 2007 *Phys. Rev.* E **76** 023708
[24] Kayser R F and Raveché H J 1978 *Phys. Rev.* A **17** 2067
[25] Mulder B M 1989 *Phys. Rev.* A **39** 360
[26] Herzfeld J, Berger A E and Wingate J W 1984 *Macromolecules* **17** 1718
[27] Odijk T and Lekkerkerker H N W 1985 *J. Phys. Chem.* **89** 2090
[28] Frenkel D and Smit B 2001 *Understanding Molecular Simulation* (San Diego, CA: Academic)

[29] Landau D P and Binder K 2000 *A Guide to Monte Carlo Simulations in Statistical Physics* (Cambridge: Cambridge University Press)
[30] Virnau P and Müller M 2004 *J. Chem. Phys.* **120** 10925
[31] Vink R L C, Wolfsheimer S and Schilling T 2005 *J. Chem. Phys.* **123** 074901
[32] Vollmayr K, Reger J D, Scheucher M and Binder K 1993 *Z. Phys.* B **91** 113
[33] Binder K and Landau D P 1984 *Phys. Rev.* B **30** 1477
[34] Borgs C and Kotecky R 1990 *J. Stat. Phys.* **61** 79
[35] Eppenga R and Frenkel D 1984 *Mol. Phys.* **52** 1303
[36] Bramwell S T and Holdsworth P C W 1994 *Phys. Rev.* B **49** 8811
[37] Binder K 1982 *Phys. Rev.* A **25** 1699
[38] Mladek B M, Gottwald D, Kahl G, Neumann M and Likos C N 2006 *Phys. Rev. Lett.* **96** 045701
[39] Glaser M A, Grason G M, Kamien R D, Košmrlj A, Santangelo C D and Ziherl P 2007 *Europhys. Lett.* **78** 46004
[40] Vink R L C 2007 *Preprint* 0706.2424
[41] Lekkerkerker H N W and Stroobants A 1994 *Nuovo Cimento* D **16** 949
[42] Wu F Y 1982 *Rev. Mod. Phys.* **54** 235
[43] Borgs C and Janke W 1992 *J. Physique* I **2** 2011